Internal Solitary Wave-Induced Bed Failure in a Stratified Water Column

Gustavo Rivera-Rosario, Peter J. Diamessis and James T. Jenkins

School of Civil and Environmental Engineering,
Cornell University
gr327@cornell.edu

Abstract

The induced-pressure over a porous bed due to the presence of an internal solitary wave (ISW) of depression is examined using numerical simulations. The bottom pressure perturbation of the propagating wave and ensuing benthic response drive sediment motion and adversely impacts the stability of any bottom-lodged structure. Assuming a two-layer, continuously stratified water column, the wave velocity and density fields can be obtained by solving the Dubreil-Jacotin-Long (DJL) Equation. The total wave-induced pressure in the water column is then computed by integrating for the hydrostatic and nonhydrostatic components. The bed is assumed to be a continuum consisting of either sand or silt with a small amount of trapped gas. Results indicate that changes in pore-water pressure penetrate deeper in the beds with more conductive materials and remains for a prolonged period long after the wave has passed. Consequently, less conductive materials hinder penetration giving rise to steeper pressure gradients. A failure criterion, comparing the vertical pressure gradient to the submerged particle weight suggests that the gradient of lowly conductive materials is strong enough to induce failure. These observations imply that the ISW-induced pressure plays a key role in the formation of powerful resuspension events observed in the field.

1 Introduction

Internal solitary waves (ISWs) are often generated by the interaction of tidal forcing acting with bathymetry and are capable of inducing significant pressure in the water column and seafloor during their propagation. They are ubiquitous oceanic phenomena typical of stratified environments. Locations of ISW observation include the South China Sea (Lien et al., 2005), Massachusetts Bay (Butman et al., 2006), Monterey Bay Shelf (Carter et al., 2005), New Jersey's Shelf (Moum and Nash, 2008) and the northwest Portuguese Shelf (Quaresma et al., 2007). The range of depths over which ISWs occur varies substantially and, consequently, so does the wave-induced bed response. Understanding the wave-bed interaction is of interest for sediment resuspension and possibly the integrity of bottom-lodged structures (Nataraja and Gill, 1983).

Observations in coastal environments as well as laboratory experiments and numerical simulations have proven the existence of wave-induced bed failure but only in the context of surface waves. The canonical flows considered in the lab include a train of waves (Scholtès et al., 2014) and the passage of the wave trough of a progressive surface wave (Sakai et al., 1992). Simulations have considered solitary surface waves (Liu et al., 2007), also in the presence of trapped gas or air in the bed. These authors' conclusions were based on a strong induced horizontal pore-pressure gradient and, to an extent, a strong vertical pore-pressure gradient provided the progressive wave trough was deep enough over an unsaturated bed (Sumer, 2014). ISW's of depression, characterized by a negative induced pressure, not only meet this criterion but also induce significant seepage (Olsthoorn et al.,

2012) and possibly a strong enough vertical pressure gradient capable of bed failure in the context of momentary liquefaction. Thus, the present work seeks to investigate the ISW-induced bottom pressure field and the potentially induced bed failure. The presentation strictly adheres to the interaction between the wave-induced pressure and the underlying bed in the absence of a background current as modeled with a high-order numerical scheme. The primary objective is to describe what are the key wave properties and bed constituents that result in failure. Subsequently, the dependence on the water depth can be addressed along with the effects of the free-surface displacement induced pressure.

2 Methodology

Water Column and Wavefield

Figure 1 illustrates both the water column and the porous medium in the model computational domain. On the water side, a two-layer continuous density stratification is assumed. The pycnocline displacement is driven by a depression wave with amplitude A, wavelength L_W, and a phase speed c. The top layer of thickness h_1 has a density ρ_1 lighter than the bottom layer h_2 with density ρ_2. The bed is described as a uniform layer of either either sand or silt with thickness L_η.

The wavefield velocity and density fields are calculated using the nonlinear eigenvalue solver for the Dubreil-Jacotin-Long (DJL) equation of Dunphy et al. (2011) which generates an exact solution to the incompressible Euler Equations under the Boussinesq approximation in a moving reference frame, $x-z$, with the wave. The bed is in a fixed reference frame $\xi - \eta$. Correspondingly, the wave imprints a translating boundary condition from the moving to fixed frame. Thus, for a given pycnocline location, thickness and reference density, the scaled Available Potential Energy (APE) of the ISW is prescribed as such to generate the strongest depression wave possible. Following the ISW pressure field analysis by Moum and Smyth (2006), only two components of the wave-induced pressure are considered: the hydrostatic pressure due to the wave driven density perturbation (p_{wh}) and the non-hydrostatic pressure which is a function of the vertical accelerations within the wave (p_{nh}). The total wave-induced pressure, p_T, is the summation of both p_{wh} and p_{nh}. The ISW-induced free-surface displacement, and its corresponding pressure, is not accounted for. Its influence shall be addressed separately in the discussion section due to its inherent variability which constrains an accurate quantification of the total pressure throughout any ISW events.

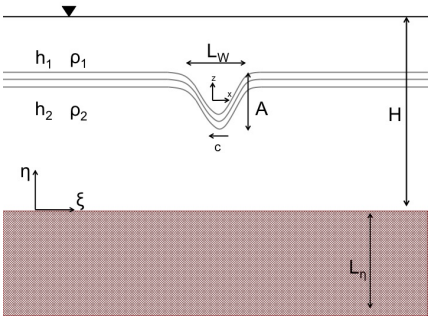

Figure 1: Problem Geometry for an ISW of depression propagating over a uniform bed of thickness L_η. The wavefield velocity and density perturbation are computed in a reference frame, $x - z$, moving with the wave. The bed lies on a fixed reference frame, ξ-η.

Bed Properties

The change in pore-water pressure is computed via (Bear, 1972),

$$\frac{k}{\rho_o g} \bigtriangledown^2 p = (\alpha + n\beta') \frac{\partial p}{\partial t} \tag{1}$$

The bed is taken to be isotropic meaning that conductivity, k, is uniform in space. Its value can be obtained from experimental data, field observations or, according to Lambe and Whitman (1969), through analytical expressions using the soil relative density and the particle diameter. The bed is assumed to be vertically confined implying that there are no horizontal displacements and that changes in the vertical are balanced by changes in the pore-water pressure (Brutsaert and El-Kadi, 1984). Thus, the bed thickness, L_η, is specified to be smaller than the ISW wavelength since the ISW represents the vertical load on the bed. In addition, a compressibility parameter, α, relating the changes in void ratio to the changes in effective stress with a porosity of $n = 0.30$ is employed which is typical of loose packing. Based on the previous assumptions, α can be expressed as a function of effective Lam*é*'s parameters as (Digby, 1981),

$$\alpha = (2\bar{\mu} + \bar{\lambda})^{-1} \tag{2}$$

Here, $\bar{\lambda}$ is Lam*é*'s effective first parameter and $\bar{\mu}$ is the effective shear modulus. Considering quartz as the main soil particle constituent, α is found to be within the range $[10^{-7}, 10^{-9}]\, 1/Pa.$ for both sand and silt. Lastly, the fluid compressibility inside the bed is considered via the parameter β', which accounts for a small amount of trapped gas. According to Verruijt (1969) and later Bear (1972), the fluid compressibility, β', is given as,

$$\beta' = \beta + \frac{1 - S_r}{p_o} \tag{3}$$

Here, S_r is the fraction of trapped gas, β is the bulk modulus of water and p_o is the absolute pore-water pressure. Based on Gratiot and Mory (2000), Tørum (2007) and Michallet et al. (2009), the oceanically representative values of S_r should be between 0.97 and 0.99. However, it is emphasized that actual field observations of how much gas is trapped at the depths considered by this study are not well documented and caution should be exercised when extrapolating values of S_r used here to the field (e.g. 50m and deeper).

3 Results

Application of the Dunphy et al. (2011) algorithm to solve the DJL equation requires supplying a pycnocline thickness δ_{pyc} and a density difference of $\Delta\rho$. The water depth is taken to be $H = 50m$, typical of continental shelf environments where nonlinear internal waves and internal solitary waves have been observed (Quaresma et al., 2007) (Moum and Nash, 2008) (Carter et al., 2005) and also where analysis of surface wave-induced liquefaction has been performed (Gratiot and Mory, 2000). The pycnocline thickness is set to $\delta/H = 0.06$ and the two-layer constant density ratio is set to $h_1/h_2 = 1/7$ typical of stratified oceanic environments. Consistent with the Boussinesq approximation, the density jump across the two-layer setting is specified as $\Delta\rho = 40\ kg/m^3$ with a reference density value of $\rho_o = 1020\ kg/m^3$. This parameters yield an ISW with an amplitude of $A = 17$m, a phase speed of $c = 2$m/s and a wavelength of $L_W = 140$m. With the obtained wave-induced velocity and density fields, the hydrostatic and non-hydrostatic pressures are

computed via trapezoidal integration using Matlab's *trapz* which is spectrally accurate for the Fourier grid of the DJL solver. The total pressure at the bottom of the water column, p_b, is taken to be the pressure at the top of the bed as enforced by assuming a one-way coupling between the wave-induced field and pore-water pressure changes. Lastly, Table 1 presents the bed classification based on the particle diameter and the corresponding conductivity for this study.

Table 1: Properties of the bed

Material	**d**(μm)	**k** (m/s)
Medium Sand	200	8.0e-5
Fine Sand	100	2.0e-5
Coarse Silt	40	3.2e-6
Medium Silt	20	8.0e-7

The simulated ISW wave-induced pressure is shown in Figure 2 for a partially saturated bed composed of medium-sized sand. The pressure has been nondimensionalized by the hydrostatic component: $p^+ = p/\Delta\rho g A$. Additionally, the streamwise coordinate has been nondimensionalized by the wavelength, $\xi^+ = \xi/L_W$, and the vertical coordinate is nondimensionalized by the wave amplitude, $\eta^+ = \eta/A$. While the wave is propagating from right to left in the water column, it leaves a diffusive imprint similar to that described by Liu et al. (2007) under solitary surface-waves. The changes in pore-water pressure do not just penetrate deeper into the bed but also linger once the wave has passed by. This lag was first studied by Yamamoto et al. (1978) under progressive surface waves and is typical of porous medium with a soil compressibility comparable to that of the fluid.

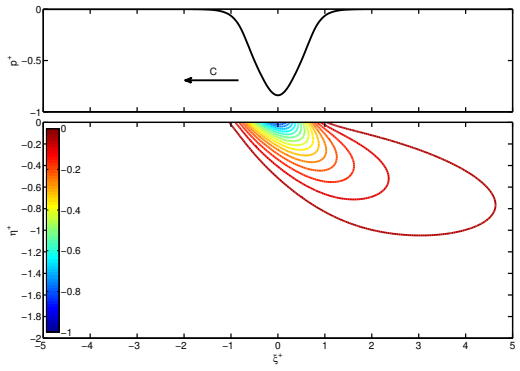

Figure 2: Contour of the nondimensional wave-induced pressure for a bed composed of medium sand for a traveling ISW with celerity $c = 2$m/s. The simulation has been performed with grid of $[N_\xi, N_\eta] = [2048,133]$ with domain dimensions: $L_\xi = 8$km and $L_\eta = 30$m. The total pressure at the bottom of the water column is included in the top figure. As the wave travels, a lag of the induced pressure occurs due to the unsaturated nature of the bed.

The change in pore-water pressure in the bed is shown in both Figure 3(a) and Figure 3(b) right under the wave trough (i.e. $\xi^+ = 0$ at Figure 2). Medium sand to medium silt with a saturation of $S_r = 0.99$ and $S_r = 0.97$ are considered with the rest of the bed properties found in Table 1. As observed in both figures, weakly conductive materials impede pore-water pressure transmission further into the bed. If the soil saturation is reduced to $S_r = 0.97$, as observed in Figure 3(b), increments in the concentration of trapped gas increase the build up for all materials giving rise to steeper gradients. Thus, for lowly conductive materials (i.e. silts) the pore-pressure builds up closer to the top of the bed causing an increase in the vertical pressure gradient.

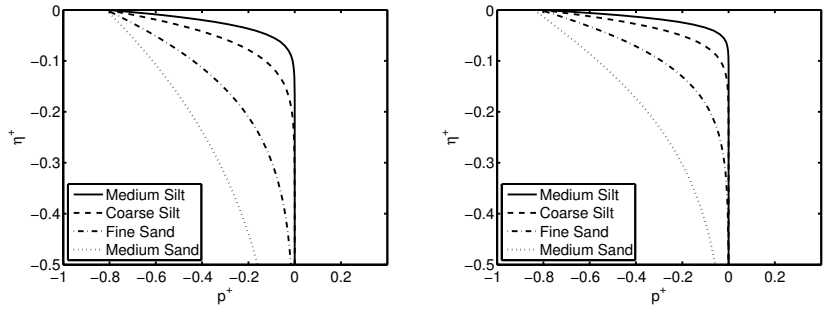

(a) (b)

Figure 3: Variation of the pore-water pressure, p^+, for a soil saturation of (a) $S_r = 0.99$ and (b) $S_r = 0.97$ as a function of depth. The composition of the bed changes from medium sand to medium silt. At lower saturation values, pore-water pressure changes do not penetrate deeper into the bed giving rise to steep gradients close to the top. The properties of the bed are included in Table 1.

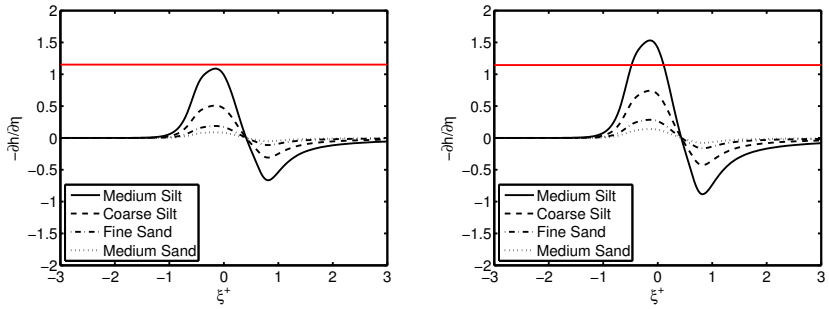

(a) (b)

Figure 4: Hydraulic gradient and submerged particle weight for a soil saturation of (a)$S_r = 0.99$ and (b)$S_r = 0.97$. The changes in pore-pressure build up with less conductive materials (see Table 1) resulting in potential bed failure as the values crosses the submerged particle weight (red line).

Following the observations of pore-water pressure build up, the role of the vertical pressure gradient is now explored. It is a measure of vertical seepage within the bed and consequently of possible failure. The vertical pressure gradient can be used to compute the hydraulic gradient at the top of the bed and compare it against the submerged particle weight ratio for unsaturated beds (γ_s'/γ_l) where γ_s' denotes the specific submerged weight of the solid and γ_l denotes specific weight of the fluid (Lambe and Whitman, 1969). Therefore, the hydraulic gradient at the top is obtained by nondimensionalizing the vertical pressure gradient with γ_l. Thus, bed failure due to this gradient occurs if

$$-\frac{\partial h}{\partial \eta} \geq \frac{\gamma_s'}{\gamma_l} \tag{4}$$

The significance of the hydraulic gradient can be understood in the context of vertical seepage in the bed. The maximum seepage is expected to occur where the pressure gradient is at a minimum. This is observed in Figure 4(a) and Figure 4(b) where the hydraulic gradient for each type of bed material is presented at different saturation values. Furthermore, the along-wave position where the magnitude of the hydraulic gradient is located indicates that subsequent onset of vertical seepage begins before the trough has passed (i.e. $\xi^+ \approx -0.5$). Seepage continues until the critical gradient decreases after the

wave trough. As observed, when the soil saturation is decreased from $S_r = 0.99$ to $S_r = 0.97$, the gradient is strong enough to overcome the submerged particle weight and to potentially cause bed failure.

4 Discussion

ISW's propagate in a range of depths varying from location to location. The applicability of the results presented in the previous section are best understood by varying water depth rather than only bed properties. Using the same criterion for bed failure, a range of test cases has been examined to evaluate potential bed failure in deeper settings. Figure 5 shows the results considering a range of two-layer constant-density layer ratios $h_1/h_2 = 1/3, 1/5, 1/7$ and $1/10$ for both saturation values using the maximum possible ISW amplitude.

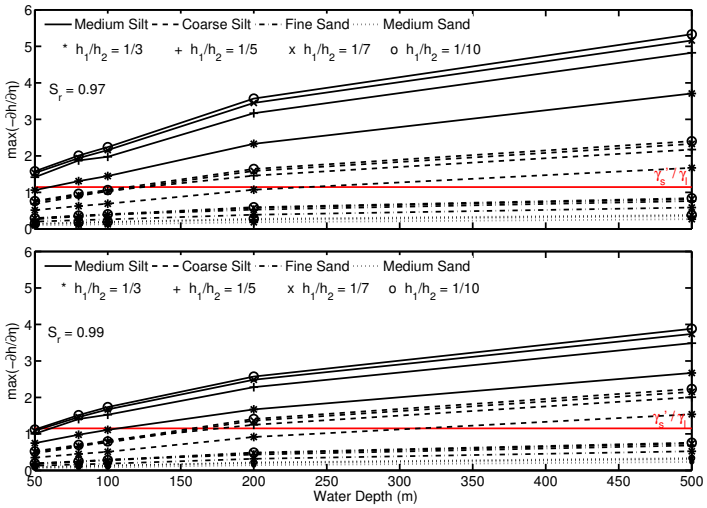

Figure 5: Maximum hydraulic gradient $\partial h/\partial \eta$ as a function of the water column depth for each type of bed component. The maximum ISW amplitude has been use across all two-layer constant density ratio h_1/h_2. The top figure corresponds to a saturation value of $S_r = 0.97$ while the bottom figure corresponds to a saturation value of $S_r = 0.99$. The submerged specific weight is shown in red.

The increase in wave-induced pressure associated with deep-water ISW's is enough to induce failure for lowly conductive materials regardless of the bed saturation. In addition, it can be noticed that all constant density layer ratios are above the specific weight of the bed for lowly conductive materials indicating that failure is not dependent on pycnocline location. If the free-surface induced pressure due to an ISW is considered, then the total pressure is reduced as it counteracts the hydrostatic pressure associated with the wave-driven disturbance. According to Moum and Smyth (2006), the free-surface induced pressure can be estimated from the horizontal ISW-induced velocity at the surface. Thus, the total pressure at the bottom of the water column is adjusted to reflect the summation of the hydrostatic pressure and the free-surface induced pressure. Similarly to the analysis in Section 3, the dependence on the free-surface induced pressure is considered and presented in Figure 6. Only the two-layer constant density ratio $h_1/h_2 = 1/7$ is considered. As observed from Figure 6, the effects are quite significant and for

$H = 50m$ only with the increment in the degree of saturation it is enough to possibly cause failure only for lowly conductive materials. However, as the water depth is increased the possibility of failure also increases and consequently at depths $H \geq 100m$ the effects of free-surface induced pressure are not large enough to prevent failure. Hence, the free-surface induced pressure, if present, can be significant enough for the passage of an ISW of depression to not cause bed failure but only at shallow depths (i.e. $H < 100m$).

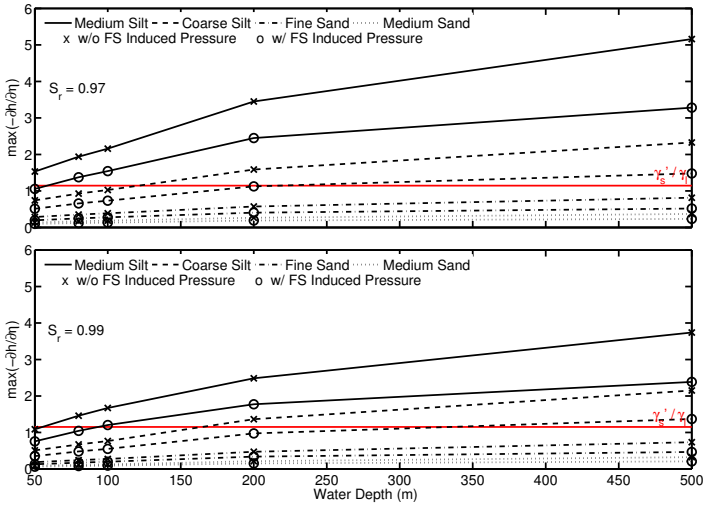

Figure 6: Maximum hydraulic gradient $\partial h/\partial \eta$ as a function of the water column depth for each type of soil with and without free-surface induced pressure. The maximum ISW amplitude has been used for a two-layer constant density ratio $h_1/h_2 = 1/7$. The top figure corresponds to a saturation value of $S_r = 0.97$ while the bottom figure corresponds to a saturation value of $S_r = 0.99$. The submerged specific weight is shown in red.

5 Conclusions

The interaction between the internal solitary wave-induced bottom pressure and the associated bed response has been explored. The total wave-induced pressure considered is a summation of both the hydrostatic and non-hydrostatic components. ISW's are capable of inducing bed failure in the context of soil liquefaction due to their inherent negative pressure. Results also indicate that failure is independent of the pycnocline location further supporting ISW contribution to the bottom sediment transport processes mentioned in the introduction. If the free-surface displacement induced pressure is not taken into accoung, the possibility of failure is reduced across all bed types and saturation values. At the continental shelf depths (i.e. $H < 100m$) only silts with a significant amount of trapped gas met the failure criteria. Deep-water ISW's (i.e. $H \geq 100m$) are still capable of inducing failure for silt beds regardless of the saturation.

References

Bear, J. (1972). *Dynamics of Fluids in Porous Media*. Elesevier.

Brutsaert, W. and El-Kadi, A. I. (1984). The relative importance of compressibility and partial saturation in unconfined groundwater flow. *Water Resources Research*, 20(3):400–408.

Butman, B., Alexander, P., Scotti, A., Beardsley, R., and Anderson, S. (2006). Large internal waves in massachussetts bay tranposrt sediments offshore. *Continental Shelf Research*, 26:2029–2049.

Carter, G., Gregg, M., and Lien, R. (2005). Internal waves, solitary-like waves, and mixing on the monterey bay shelf. *Continental Shelf Research*, 25:1499–1520.

Digby, P. (1981). The effective elastic moduli of porous granular rock. *Journal of Applied Mechanics*, 48:803–808.

Dunphy, M., Subich, C., and Stastna, M. (2011). Spectral methods for internal waves: indistinguishable density profiles and double-humped solitary waves. *Nonlinear Processes in Geophysics*, 18:351–358.

Gratiot, N. and Mory, M. (2000). Wave-induced sea bed liquefaction with application to mine burial. In *Proceedings of the Tenth (2002) International Offshore and Polar Engineering Conference*.

Lambe, T. and Whitman, R. (1969). *Soil Mechanics*. John Wiley and Sons, Inc.

Lien, R.-C., Yang, T., Chang, M., and D'Asaro, E. (2005). Energy of nonlinear internal waves in the south china sea. *Geophysical Research Letters*, 32(L05615).

Liu, P., Park, Y., and Lara, J. (2007). Long-wave-induced flows in an unsaturated permeable bed. *Journal of Fluid Mechanics*, 586:323–345.

Michallet, H., Mory, M., and Piedra-Cueva, I. (2009). Wave-induced pore pressure measurements near a coastal structure. *Journal of Geophysical Research*, 114(C06019):1–18.

Moum, J. and Nash, J. (2008). Seafloor pressure measurements of nonlinear internal waves. *Journal of Physical Oceanography*, 38:481–491.

Moum, J. and Smyth, W. (2006). The pressure disturbance of a nonlinear internal wave train. *Journal of Fluid Mechanics*, 558:153–177.

Nataraja, M. and Gill, H. (1983). Ocean wave-induced liquefaction analysis. *Journal of Geotechnial Engineering*, 109(4):573–590.

Olsthoorn, J., Stastna, M., and Soontiens, N. (2012). Fluid circulation and seepage in lake sediment due to propagating and trapped internal waves. *Water Resources Research*, 48.

Quaresma, L., Vitorino, J., Oliveira, A., and da Silva, J. (2007). Evidence of sediment resuspension by nonlinear internal waves on the western portuguese mid-shelf. *Marine Geology*, 246:123–143.

Sakai, T., Hatanaka, K., and Mase, H. (1992). Wave-induced effective stress in seabed and its momentary liquefaction. *Journal of Waterway, Port, Coastal and Ocean Engineering*, 118(2):202–206.

Scholtès, L., Chareyre, B., Michallet, H., Catalano, E., and Marzougui, M. (2014). Modeling wave-induced pore pressure and effective stress in a granular seabed. *Continuum Mechanics and Thermodynamics*, 27(1):305–323.

Sumer, M. (2014). *Liquefaction Around Marine Structures*. World Scientific.

Tørum, A. (2007). Wave-induced pore pressure- air/gas content. *Journal of Waterway, Port, Coastal, and Ocean Engineering*, 133(1):83–86.

Verruijt, A. (1969). *Flow Through Porous Media*, chapter Elastic Storage of Aquifers. Academic Press.

Yamamoto, T., Koning, H., Sellmeijer, H., and Van Hijum, E. (1978). On the response of a poro-elastic bed to water waves. *Journal of Fluid Mechanics*, 87:193–206.